Marshall, R. Kobayashi, *Am. Inst. Chem. Eng. J.* **10**, 734 (1964); also see (*13*), p. 54.]

13. *Handbook of Gas Hydrate Properties and Occurrence* (U.S. Dept. of Energy Publication DOE/MC/19239-1546, 1983).
14. Exceptions were those samples that leaked *P* at warm *T* to either prevent full reaction or to cause partial dissociation of clathrate to CH_4 gas + H_2O liquid. After refreezing, these samples showed obvious melt textures; they displayed an outer cylindrical ring of clear, nonporous ice, with cloudy, gas-charged ice concentrated in the center of the sample as the freezing front progressed from the outside to the interior. Partially dissociated samples also showed large amounts of ice in their XRD patterns. Additional evidence of melting was provided by the loosely fitting top disk (Fig. 2). In samples that leaked *P*, the disk was found to drop to a midpoint in the molding tube as residual seed ice melted. In fully reacted samples, however, the disk remained at the top of the sample.
15. Only H_2, He, and Ne are too small to form clathrates at our test conditions; we chose Ne because it is the largest of these and hence the easiest to seal.
16. The clathrate-forming reaction CH_4 (g) + $6H_2O$ (ice) → $CH_4{\cdot}6H_2O$ liberates a small amount of latent heat {$\sim$20 ± 0.3 kJ/mol at 273 K and a CH_4 pressure of 28 MPa, as determined from the Clapeyron slope [T. Makogon and E. Sloan, *J. Chem. Eng. Data* **39**, 2, 351 (1994)], the measured enthalpy of formation at standard conditions [Y. Handa, *Chem. Thermodyn.* **18**, 915 (1986)], the reaction volume change (*11*), and its variation with pressure (*13*)}. This heat is not reflected as a sample *T* anomaly (Fig. 3B, inset), evidently because the clathrate reaction occurs over 8 hours and such heat would be small compared with the exchange of heat by conduction of the sample with its surroundings. The standard enthalpy for melting H_2O ice is −6.01 kJ/mol, or −36.07 kJ/6.1 mol for comparison with the clathrate-forming reaction.
17. This curve was calculated from the melting behavior of ice measured in Ne runs and assumes that (i) the seed ice grains melted as the ice did in the Ne run, (ii) changes in CH_4 *P* scale with Ne *P* changes through the Ne and CH_4 equations of state, and (iii) solubility of Ne in H_2O is negligible. The magnitude of the *P* drop was verified independently from the CH_4 equation of state.
18. P. Villard, *C. R. Assoc. Fr. Avanc. Sci.* **106**, 1602 (1888). See also (*2*, *9*).
19. Hwang *et al.* (*9*) note that because hydrate formation is an exothermic process, heat released by the phase change during crystallization increases the *T* at the formation interface. This effect is greater for hydrate formation from liquid H_2O than from ice because the heat of formation is partially absorbed by the melting ice.
20. Conceptual models of hydrate growth by diffusion have been discussed previously [Y. Makogon, *Hydrates of Natural Gases*, W. H. Cielewicz, Transl. (PennWell, Tulsa, OK, 1981)] and later by Hwang *et al.* (*9*).
21. Superheating has been measured in gold-plated silver single crystals [J. Daeges, H. Gleiter, J. Perepezko, *Phys. Lett.* **119A**, 79 (1986)], and results suggest that either a free external surface or internal defects or dislocations are critical for melting to take place at the normal melting point [S. Phillpot, J. Lutsko, D. Wolf, S. Yip, *Phys. Rev. B* **40**, 2831 (1989); see also S. Phillpot, S. Yip, D. Wolf, *Comput. Phys.* **3**, 20 (1989). In the present study, we detected no clathrate formation during the initial *T* run-up to 271.5 K (*10*), when the sample is in the ice sub-solidus field, and hence we have ruled out the liklihood that a rind of clathrate encased the ice grains before they were warmed above the H_2O liquidus. It remains possible, however, that such a microlayer actually formed but was at or below our XRD detection levels.
22. Also, methane hydrate crystallization from a bulk liquid H_2O phase is difficult to initiate because of the low solubility of the gas in the bulk liquid (*2*, *9*).
23. Several investigators have reported demonstrating the phenomenon of superheating ice with respect to the vapor phase [E. Roedder, *Science* **155**, 1413 (1967); G. Schubert and R. E. Lingenfelter, *ibid.* **168**, 469 (1970); see also discussion by B. Kamb, *ibid.* **169**, 1343 (1970)] or with respect to the liquid phase, M. Kåss and S. Magun [*Z. Kristallogr.* **116**, 354 (1961)]. See also C. Knight and A. DeVries, *Science* **245**, 505 (1989).
24. H. Heard, W. Durham, C. Boro, S. Kirby, in *The Brittle-Ductile Transition in Rocks, Geophysical Monograph* 56, A. Duba *et al.*, Eds. (American Geophysical Union, Washington, DC, 1990), pp. 225–228. In our experiments, piston force and displacement rate were recorded, corrected for instantaneous sample area and length changes, and converted to differential stress (σ), axial shortening strain (ε), and strain rate ($\dot{\varepsilon}$).
25. W. Durham, S. Kirby, L. Stern, *J. Geophys. Res.* **97**, E12, 20883 (1992); S. Kirby, W. Durham, M. Beeman, H. Heard, M. Daley, *J. Phys.* **48** (suppl.), 227 (1987).
26. During hydrostatic compaction, confining *P* was slowly "stepped" up to 100 MPa in increments of about 20 MPa. After each *P* step, the piston was advanced to touch and square the bottom of the sample, then advanced just sufficiently to lightly compress the sample in order to compact it with minimal plastic deformation. Six of the samples were compacted by means of an internal vent line to eliminate the pore-space gas, and two of the samples were compacted without the venting capability. The two nonvented samples (281 and 282; Table 1) showed equally large fractions of ice in their post-deformation x-ray patterns as the vented samples.
27. Indium jacket replicas of deformed sample surfaces showed evidence of heterogeneous ice precipitation. Areas with exsolved ice appear on jackets of all deformed samples as discrete patches with noticeably finer grain size than the surrounding clathrate.
28. We thank B. Kamb, J. Kargel, K. Kvenvolden, and W. McKinnon for critically reviewing the manuscript and for helpful discussions. This work was supported under NASA order W-18,927 and was performed in part under the auspices of the U.S. Department of Energy by the Lawrence Livermore National Laboratory under contract W-7405-ENG-48.

29 April 1996; accepted 10 July 1996

A Trinuclear Intermediate in the Copper-Mediated Reduction of O_2: Four Electrons from Three Coppers

Adam P. Cole, David E. Root, Pulakesh Mukherjee,
Edward I. Solomon, T. D. P. Stack*

The reaction of metal complexes with dioxygen (O_2) generally proceeds in 1:1, 2:1, or 4:1 (metal:O_2) stoichiometry. A discrete, structurally characterized 3:1 product is presented. This mixed-valence trinuclear copper cluster, which contains copper in the highly oxidized trivalent oxidation state, exhibits O_2 bond scission and intriguing structural, spectroscopic, and redox properties. The relevance of this synthetic complex to the reduction of O_2 at the trinuclear active sites of multicopper oxidases is discussed.

The copper-mediated activation of O_2 plays a vital role in biological and synthetic oxidative catalysis (*1*–*4*). Recent investigations of O_2 reduction with Cu(I) complexes have shown that Cu is remarkably versatile regarding both the degree of reduction and the coordination mode of the reduced O_2 species. Reductions to superoxide (*2*, *5*), peroxide (*2*, *3*, *6*, *7*), and water (*2*) involving one, two, and four electrons (e^-), respectively, have been documented, in which each Cu(I) supplies one electron. The variety of Cu sites found in natural enzymes that bind or activate O_2 reflects this versatility. The Cu enzymes responsible for the $4e^-$ reduction of O_2 to H_2O—laccase, ceruloplasmin, and ascorbate oxidase—each contain a trinuclear Cu active site (*8*–*12*) with an additional mononuclear "blue" Cu site 12 Å distant (*9*). The known binuclear Cu proteins hemocyanin and tyrosinase (*3*, *6*) bind O_2 through $2e^-$ reduction to $O_2{}^{2-}$, but the fully reduced trinuclear site is the minimal structural subunit required for biological O_2 bond cleavage and reduction to H_2O (*8*, *13*).

A self-assembly approach to the synthesis of a bi- or trinuclear Cu-O_2 cluster from monomeric Cu(I) complexes and O_2 assumes facile assembly and thermodynamic stability of the resulting product under the reaction conditions. Accordingly, the use of simple ligands is an appropriate strategy. A number of monomeric 1:1 Cu(I):*N*-peralkylated-diamine complexes were examined by manometry for 3:1 Cu:O_2 reactivity. Structural and spectroscopic studies of the oxidation of one such Cu(I) complex (**1**) demonstrate the formation of a trinuclear intermediate (**2**) in the Cu(I)-mediated reduction of O_2 whose 3:1 stoichiometry is unprecedented not only in the case of Cu but among all discrete metal-O_2 reactions (Scheme 1, Me = methyl). Its structural, spectroscopic, and redox properties indicate that, in the process of O_2 bond cleavage, the three Cu(I) sites in **2** are oxidized by a total of four electrons, forming a mixed-valence cluster with bridging oxide ligands that stabilize one of the Cu sites in its normally inaccessible

---

Department of Chemistry, Stanford University, Stanford, CA 94305, USA.

*To whom correspondence should be addressed.

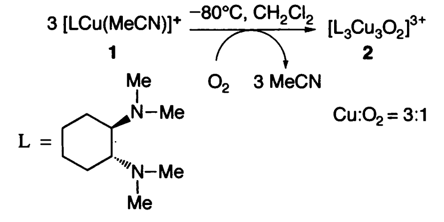

Scheme 1.

trivalent oxidation state.

N-Permethylated (1*R*,2*R*)-cyclohexanediamine (L) (*14*) stabilizes Cu(I) as a mononuclear, trigonal-planar complex with MeCN as a labile auxiliary (*15*) (**1**). The reaction of **1** with excess O_2 is extremely sensitive to temperature and solvent and is performed at atmospheric pressure in cold (−80°C), purified CH_2Cl_2 (*16*). Manometric measurements indicate that sufficiently concentrated (>10 mM) solutions (*17*) of [**1**](OTf) ($OTf^- = C_3SO_3^-$) absorb one-third of an equivalent (equiv) of O_2 (*18*) to yield a dark brown species (**2**) formulated as $[L_3Cu_3O_2](OTf)_3$, which displays intense ultraviolet absorption bands (Fig. 1). As **1** cannot be regenerated from **2** by displacement with gaseous CO, by PPh_3 (Ph, phenyl), or by any combination of evacuation and heating, O_2 binding is effectively irreversible. Once formed, $[\mathbf{2}](OTf)_3$ exhibits moderate thermal stability, decomposing by a non–first-order process in about 3 hours at −10°C. In the presence of trace H_2O, the major isolated product is the bis(μ_2-hydroxo) dicopper (II) dimer $[L_2Cu_2(OH)_2](OTf)_2$ (*19*).

Thermally sensitive crystals of $[\mathbf{2}](OTf)_3$ were characterized by x-ray diffraction (*20*). The unit cell contains two crystallographically distinct (*21*) trinuclear $[L_3Cu_3O_2]$ clusters (Fig. 2A) in which the O-O bond has been broken (O···O distance = 2.37 Å) (Fig. 2B). The three monoanions associated with each trinuclear unit establish an overall charge of 3+ per cluster. The $[Cu_3O_2]$ core is nearly trigonal bipyramidal, with the O atoms occupying the axial positions; however, it does not possess threefold symmetry (*22*). Instead, each cluster resides on a crystallographic twofold axis that perpendicularly bisects the vector between the O atoms, passing through one Cu atom and relating the remaining pair. Each Cu is ligated by two amine N atoms and two O atoms in a square planar geometry; however, the unique Cu site (Cu2, Fig. 2) of each cluster exhibits unusually short Cu-O bond distances (1.84 Å) that are at least 0.15 Å shorter than the other Cu-O bond distances (Fig. 2B), indicative of a higher relative oxidation level. Similar Cu-O bond lengths have been reported for the solid-state material $KCu^{III}O_2$ (1.84 Å) (*23*), which forms an extended square planar $[CuO_{4/2}]_n$ lattice, and more recently for the dimeric $[(Bn_3TACN)_2Cu_2O_2](SbF_6)_2$ (1.81 Å) (*17*). Because the bridging O ligands in **2** are common to all three metals, the observed bond length inequivalence must be predominantly due to the unique Cu. The structure is consistent with the formal description of **2** as a mixed-valence cluster consisting of two Cu(II) ions and a single Cu(III), bridged by two μ_3-oxo ligands (*24*).

Nuclear magnetic resonance (NMR) susceptibility measurements (*25*) performed on concentrated (30 mM) solutions of **2** at 183 K indicate a magnetic moment (μ_{eff}) of 2.9(1) Bohr magnetons (number in parentheses is the standard deviation in the last digit). For polycrystalline solid samples at 1.6 K, the variable-field saturation magnetization behavior of magnetic circular dichroism (*26*) transitions associated with an ultraviolet absorption feature of **2** (Fig. 1) indicates a ferromagnetically coupled triplet (spin $S = 1$) ground state. In conjunction with its solid-state structure, these magnetic properties of **2** support an electronic description in which the two $S = ½$ Cu(II) atoms are ferromagnetically coupled, whereas the Cu(III) site is diamagnetic (low spin d^8) because of its square planar coordination and strong ligand field (*27*). The absorption spectrum of **2** contains intense bands between 280 and 380 nm (Fig. 1) that are attributed to oxide-to-Cu(III) ligand-to-metal charge transfer (LMCT) on the basis of their relatively low energy. The high intensity of these LMCT spectral features indicates a significant degree of covalency in the Cu(III)-O bond (*28*).

Copper(III) complexes are generally strong oxidants, but their potential is significantly influenced by ligation geometry and solvation. A square planar, anionic coordination environment that inhibits axial interactions will favor the d^8 Cu(III) oxidation state; reduction potentials near 0 V versus a standard calomel electrode have been reported for such complexes (*29*). Accordingly, although treatment of **2** at −80°C with ferrocene (reduction potential $E_{1/2} = 0.48$ V) (*30*) quenches its characteristic optical absorptions, **2** fails to react with the more oxidatively resistant acetylferrocene ($E_{1/2} = 0.79$ V) (*31*), placing its potential between these values. Spectrophotometric titration of **2** with 1 equiv of 2,4-di-*tert*-butylphenol in the absence of O_2 yields the 6,6′-coupled product (3,3′,5,5′-tetra-*tert*-butyl-2,2′-biphenol) quantitatively. In this reaction, **2** acts as both $1e^-$ oxidant and proton acceptor.

The assembly of **2** at low temperature indicates that the $[Cu_3O_2]$ core is an enthalpically preferred arrangement in an aprotic environment. Stabilization of the Cu(III) center is attributed to favorable covalent bonding interactions with the oxide ligands and to the optimal square planar coordination achieved

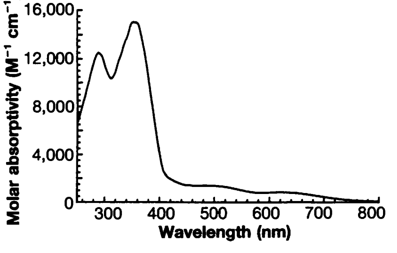

Fig. 1. Ultraviolet-visible spectrum of $[\mathbf{2}](OTf)_3$ (30 mM) in CH_2Cl_2 at −80°C (ε = 12,500 M^{-1} cm^{-1} at λ_{max} = 290 nm, 15,000 M^{-1} cm^{-1} at 355 nm, 1400 M^{-1} cm^{-1} at 480 nm, and 800 M^{-1} cm^{-1} at 620 nm).

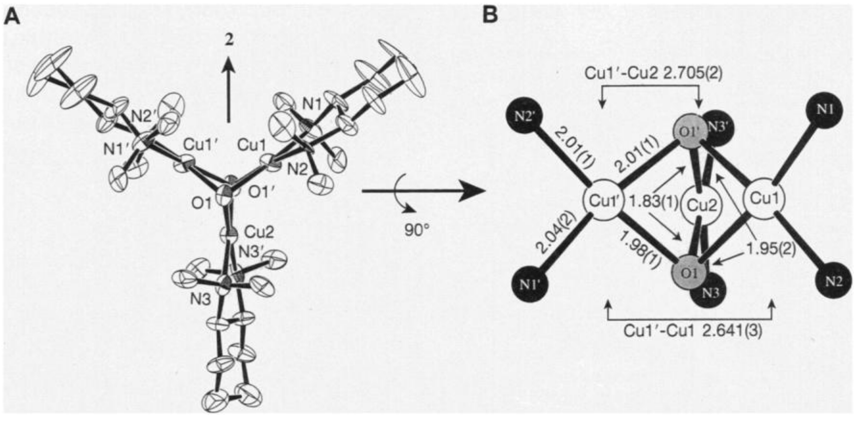

Fig. 2. (**A**) ORTEP representation (50% probability), atom-labeling scheme (unlabeled ellipsoids represent carbon atoms). (**B**) $[N_6Cu_3O_2]$ core metrical parameters showing interatomic distances (in angstroms) for one $[L_3Cu_3O_2]^{3+}$ cluster (**2**). The view is oriented down the crystallographically imposed twofold axis on which Cu2 resides. Selected interatomic distances (in angstroms): Cu1-Cu2, 2.641(3); Cu1-Cu1′, 2.704(3); O1-O1′, 2.37; N1-N2, 2.86; and N3-N3′, 2.73. Selected angles (in degrees): O1-Cu1-O1′, 72.6(6)°; O1-Cu2-O1′, 80.4(8)°; Cu1-O1-Cu1′, 85.3(5)°; and Cu1-O1-Cu2, 86.7(5)°.

by each Cu within the $[Cu_3O_2]$ core. Upon inspection of the crystal structure of the fully reduced form of ascorbate oxidase (*11*), the three trigonally ligated Cu(I) centers (average Cu···Cu distance, 4.5 Å) appear geometrically predisposed toward accommodation of O_2 and formation of a $[Cu_3O_2]$ cluster. However, no current spectroscopic studies of the metastable oxygen intermediates of multicopper oxidases and their derivatives support the existence of an intensely absorbing oxo-Cu(III) chromophore, and no unusually short Cu-O bond distances such as those observed in **2** are indicated (*12, 13, 32*). In accordance with these studies, however, the facile reaction of three Cu(I) monomers with O_2 to form the mixed-valence bis(μ_3-oxo)[Cu(II)Cu(II) Cu(III)] species **2** does suggest that O_2 bond cleavage at trinuclear Cu sites requires full $4e^-$ reduction of O_2. In the case of native laccase, the fourth electron is provided by the remote "blue" Cu center, whereas in **2**, the extra electron must be obtained at the cost of further oxidation of one of the Cu sites.

REFERENCES AND NOTES

1. K. D. Karlin and Z. Tyeklár, Eds., *Bioinorganic Chemistry of Copper* (Chapman & Hall, New York, 1993).
2. N. Kitajima and Y. Moro-oka, *Chem. Rev.* **94**, 737 (1994).
3. E. I. Solomon, M. J. Baldwin, M. D. Lowery, *ibid.* **92**, 521 (1992); E. I. Solomon and M. D. Lowery, *Science* **259**, 1575 (1993).
4. K. D. Karlin and S. Fox, in *Active Oxygen in Biochemistry*, J. S. Valentine, C. S. Foote, A. Greenberg, J. F. Liebman, Eds. (Chapman & Hall, Glasgow, 1995), vol. 3, pp. 188–231.
5. K. Fujisawa, M. Tanaka, Y. Moro-oka, N. Kitajima, *J. Am. Chem. Soc.* **116**, 12079 (1994); M. Harata, K. Jitsukawa, H. Masuda, H. Einaga, *ibid.*, p. 10817.
6. K. A. Magnus, H. Ton-That, J. E. Carpenter, *Chem. Rev.* **94**, 727 (1994).
7. T. N. Sorrell, W. E. Allen, P. S. White, *Inorg. Chem.* **34**, 952 (1995); W. E. Lynch, D. M. Kurtz, S. K. Wang, R. A. Scott, *J. Am. Chem. Soc.* **116**, 11030 (1994); S. Mahapatra, J. A. Halfen, E. C. Wilkinson, L. Que, W. B. Tolman, *ibid.*, p. 9785.
8. D. J. Spira-Solomon, M. D. Allendorf, E. I. Solomon, *J. Am. Chem. Soc.* **108**, 5318 (1986).
9. A. Messerschmidt *et al.*, *J. Mol. Biol.* **224**, 179 (1992).
10. M. D. Allendorf, D. J. Spira, E. I. Solomon, *Proc. Natl. Acad. Sci. U.S.A.* **82**, 3063 (1985); L. Ryden and I. Björk, *Biochemistry* **15**, 3411 (1976); I. Zaitseva *et al.*, *J. Biol. Inorg. Chem.* **1**, 15 (1996).
11. A. Messerschmidt, H. Luecke, R. Huber, *J. Mol. Biol.* **230**, 997 (1993).
12. J. L. Cole, P. A. Clark, E. I. Solomon, *J. Am. Chem. Soc.* **112**, 9534 (1990).
13. J. L. Cole, G. O. Tan, E. K. Yang, K. O. Hodgson, E. I. Solomon, *ibid.*, p. 2243.
14. The (1*R*,2*R*)-cyclohexanediamine backbone was chosen both for its preorganized nature and its chirality. In its energetically preferred conformation with the two amine substituents equatorially positioned, this ligand is preorganized for binding a single metal. The enantiomeric purity of the ligand significantly reduces the probability of forming diastereomeric complexes.
15. Although **1** has not been structurally characterized, its ^1H NMR spectrum in the diamine ligand region is nearly identical to that of the structurally characterized trigonal planar complex $[LCu(PPh_3)](CF_3SO_3)$, which is formed upon addition of PPh_3 to a solution of **1**. The *N*-perethylated analog of **1**, $[(L')Cu(CH_3CN)](CF_3SO_3)$ [L′ = *N*,*N*,*N*′,*N*′-tetraethyl-*trans*-(1*R*,2*R*)-cyclohexanediamine], with bound CH_3CN has also been structurally characterized as a trigonal planar species (*18*).
16. Reported concentrations and molar absorptivites are uncorrected for the thermal contraction of CH_2Cl_2 at below-ambient temperatures, consistent with other reports.
17. The product of oxygenation depends on the concentration of **1**. Reaction of solutions at or below 1 mM in **1** generates a different species **X** with extremely intense electronic and vibrational transitions [per Cu atom: molar absorptivity $\varepsilon = 10{,}000\ M^{-1}\ cm^{-1}$ at wavelength $\lambda_{max} = 295$ nm, $\varepsilon = 13{,}000\ M^{-1}\ cm^{-1}$ at 392 nm; resonance Raman features at 607 and 583 cm^{-1} for $^{16}O_2$- and $^{18}O_2$-derived samples, respectively (CH_2Cl_2 solution, 407-nm excitation)]. The close spectroscopic resemblance of **X** to the structurally characterized dimer $[(Bn_3TACN)_2Cu_2O_2](SbF_6)_2$ recently reported [J. A. Halfen *et al.*, *Science* **271**, 1397 (1996)] suggests that it is a similar 2:1 Cu:O_2 complex (Bn_3TACN = 1,4,7-tribenzyl-1,4,7-triazacyclononane).
18. Supporting information is available from the author or at the *Science* Web site http://www.sciencemag. org/science/feature/beyond/#cole. Included are synthetic procedures and spectroscopic characterization data for all new compounds and x-ray structural information, including tables of crystal collection data, positional and thermal parameters, and interatomic distances and angles.
19. Isolated yield, 60%. The x-ray crystal data is available (*18*).
20. Crystal data for [**2**]·4 CH_2Cl_2: brown rhombic blocks from cold (−40°C) CH_2Cl_2-ether; monoclinic *C*2 (no. 5), $a = 28.0300(1)$ Å, $b = 16.8004(3)$ Å, $c = 15.3760(2)$ Å, $\beta = 119.158(1)°$, $V = 6323.2(1)$ Å^3, and $Z = 4$; 14,745 reflections were collected and appropriately averaged (*18*), 9779 of which were unique (150 K, $3° < 2\theta < 46°$); 7124 reflections $[|F_o| > 4\sigma(F_o)]$ yield $R = 7.4$ and $R_w = 7.6$.
21. Although the two clusters are crystallographically unique, they are isostructural to within a root-mean-square (rms) deviation of 0.162 Å (0.093 Å rms for the $N_6Cu_3O_2$ core).
22. The structure of **2** bears a strong superficial resemblance to that of a previously reported macrocyclic bis(μ_3-hydroxo)tricopper(II) species; however, this thermally stable cluster exhibits full threefold symmetry, has normal Cu(II)-O and Cu(II)-N distances, and carries an overall charge of 4+ [J. Comarmond, B. Dietrich, J. Lehn, R. Louis, *Chem. Commun.* **1985**, 74 (1985)].
23. K. Hesterman and R. Hoppe, *Z. Anorg. Allg. Chem.* **367**, 249 (1969).
24. Formulation of **2** as a μ_3-hydroxo-μ_3-oxotricopper(II) species would also be consistent with an overall charge of 3+ but fails to rationalize the short Cu-O bonds exhibited by the unique Cu site.
25. D. F. Evans, *J. Chem. Soc.* **1959**, 2003 (1959).
26. P. N. Schatz, R. L. Mowery, E. R. Krausz, *Mol. Phys.* **35**, 1537 (1978).
27. Ferromagnetic interactions in Cu_2O_2 cores have been reported previously [for example, P. Chaudhuri *et al.*, *Angew. Chem. Int. Ed. Engl.* **24**, 57 (1985)].
28. M. J. Baldwin *et al.*, *J. Am. Chem. Soc.* **114**, 10421 (1992).
29. M. P. Youngblood and D. W. Margerum, *Inorg. Chem.* **19**, 3068 (1980).
30. D. Chang, T. Malinski, A. Ulman, K. Kadish, *ibid*. **23**, 817 (1984).
31. C. LeVanda, K. Bechgaard, D. O. Cowan, M. D. Rausch, *J. Am. Chem. Soc.* **99**, 2964 (1977).
32. W. Shin *et al.*, *J. Am. Chem. Soc.* **118**, 3202 (1996); P. A. Clark and E. I. Solomon, *ibid.* **114**, 1108 (1992).

33. We thank the University of California Mass Spectrometry Facility (Department of Pharmaceutical Chemistry, San Francisco); Z. Hou and V. Mahadevan for experimental assistance; and F. Hollander for use of the Siemens SMART diffractometer at the University of California at Berkeley. Funding provided by NIH grants GM50730 (T.D.P.S.) and DK31450 (E.I.S.) and an NSF predoctoral fellowship (A.P.C.).

22 April 1996; accepted 5 August 1996

Age and Paleogeographical Origin of Dominican Amber

Manuel A. Iturralde-Vinent* and R. D. E. MacPhee

The age and depositional history of Dominican amber-bearing deposits have not been well constrained. Resinites of different ages exist in Hispaniola, but all of the main amberiferous deposits in the Dominican Republic (including those famous for yielding biological inclusions) were formed in a single sedimentary basin during the late Early Miocene through early Middle Miocene (15 to 20 million years ago), according to available biostratigraphic and paleogeographic data. There is little evidence for extensive reworking or redeposition, in either time or space. The brevity of the depositional interval (less than 5 million years) provides a temporal benchmark that can be used to calibrate rates of molecular evolution in amber taxa.

In the Dominican Republic, amber (*1*) occurs in commercially exploitable quantities in two zones (Fig. 1): north of Santiago de los Caballeros (the "northern area") and northeast of Santo Domingo (the "eastern area"). Amber from the northern area has been suggested to be as old as Early Eocene or as young as Early Miocene (*2–7*); estimates for the eastern area are more diverse, ranging from Cretaceous to Recent (*2–4, 6–9*). Age spreads of this magnitude are implausible, but to date no resolution of the age of Dominican amber has met with wide acceptance. The resolution offered here is based on a synthesis of available biostratigraphic and paleogeographic data from several parts of Hispaniola (Fig. 2).

In the eastern area, amber-bearing sedi-

M. A. Iturralde-Vinent, Museo Nacional de Historia Natural, Obispo 51, La Habana CH 10100, Cuba.
R. D. E. MacPhee, Department of Mammalogy, American Museum of Natural History, New York, NY 10024–5192, USA.

*To whom correspondence should be addressed. Present address: Department of Mammalogy, American Museum of Natural History, New York, NY 10024–5192, USA. E-mail: manuel@amnh.org